

A Quantum Inspired Bi-level Optimization Algorithm for the First Responder Network Design Problem

Anthony Karahalios^{1*}, Sridhar Tayur^{1†}, Ananth Tenneti^{1‡},
 Amirreza Pashapour², F. Sibel Salman², Barış Yıldız²
¹ Carnegie Mellon University, Pittsburgh, PA 15213, USA
² Koç University, Istanbul, 34450, Türkiye

January 24, 2024

Abstract

In the aftermath of a sudden catastrophe, First Responders (FR) strive to promptly reach and rescue immobile victims. Simultaneously, other mobile individuals take roads to evacuate the affected region, access medical facilities or shelters, or reunite with their relatives. The escalated traffic congestion significantly hinders critical FR operations if they share some of the same roads. A proposal from the Turkish Ministry of Transportation and Infrastructure being discussed for implementation is to allocate a subset of road segments for use by FRs only, mark them clearly, and pre-communicate them to the citizens. For the FR paths under consideration: (i) there should exist an FR path from designated entry points to each demand point in the network, and (ii) evacuees try to leave the network (through some exit points following the selfish routing principle) in the shortest time possible when they know that certain segments are not available to them. We develop a mixed integer non-linear programming formulation for this First Responder Network Design Problem (FRNDP). We solve FRNDP using a novel hybrid quantum-classical heuristic building on the Graver Augmented Multi-Seed Algorithm (GAMA). Using the flow-balance constraints for the FR and evacuee paths, we use a Quadratic Unconstrained Binary Optimization (QUBO) model to obtain a partial Graver Bases to move between the feasible solutions of FRNDP. To efficiently explore the solution space for high-quality solutions, we develop a novel bi-level nested GAMA within GAMA: GAGA. We test GAGA on random graph instances of various sizes and instances related to an expected Istanbul earthquake. Comparing GAGA against a state-of-the-art exact algorithm for traditional formulations, we find that GAGA offers a promising alternative approach. We hope our work encourages further study of quantum (inspired) algorithms to tackle complex optimization models from other application domains.

Keywords: Disaster Preparedness, Quantum-inspired algorithm, Quadratic Unconstrained Binary Optimization (QUBO), Graver Augmented Multi-seed Algorithm (GAMA)

1 Introduction

Disaster Management (DM) is an important (and growing) area of study in our operations research community. DM research has been stratified into four groups: mitigation, preparedness, response,

*akarahal@andrew.cmu.edu

†stayur@andrew.cmu.edu

‡vat@andrew.cmu.edu

and recovery. This paper adds to the preparedness research - pre-disaster planning for a swift and effective post-disaster response - by studying the First Responder Network Design Problem (FRNDP).

The complex and time-critical nature of response operations mandates meticulous pre-disaster planning. This proactive approach, employing analytical methodologies, is essential to facilitate the swift implementation of pre-identified (and pre-communicated) policies immediately when a disaster strikes. The two consecutive earthquakes of magnitudes 7.8 and 7.5 experienced in Türkiye on February 6, 2023, that affected over 15 million people in 11 provinces in southwestern Türkiye and northwestern Syria, exemplify the complexity of the required response operations. The earthquakes caused over 50,000 deaths, more than 100,000 injuries, and over 2.7 million displaced people in Türkiye alone due to 36,932 collapsed and more than 311,000 damaged buildings [51]. After the earthquakes, 271,060 personnel were deployed to the region, including 35,250 search and rescue personnel, public employees, personnel of NGOs, international search and rescue personnel, and volunteers [43]. Although rescue and response teams tried to reach the disaster-stricken region immediately, time lags occurred due to difficulties in accessibility, and not all cities and villages could be provided emergency services within the critical first 24 hours [34].

After a sudden-onset disaster, such as an earthquake, mobile individuals naturally attempt to evacuate the affected region, access medical facilities or shelters, and reunite with their relatives [20]. Simultaneously, first responders (FR) comprising search-and-rescue teams, firefighters, police officers, ambulance crews, debris clearance, and road restoration teams, relief aid distribution teams, and volunteers rely on the same road infrastructure to promptly reach victims in urgent need [2]. The inevitable traffic congestion caused by the mobile citizenry significantly hinders critical first-response operations.

One of the operational planning proposals to ensure the accessibility of the FRs is to reserve one or more lanes on portions of the road network exclusively for the use of FR vehicles during the crucial initial hours following a disaster also referred to as “golden hours” [30]. However, this course of action requires careful planning, as this allocation diminishes the already congested road capacity for the mobile public. Furthermore, road reservations must be decided and announced before the occurrence of a disaster. Attempting to communicate and enforce such a strategy amidst the chaos of a disaster, compounded by potential communication breakdowns, would pose an extremely challenging, if not impossible, task. Knowing which road segments should be dedicated to the FRs also has the benefit that they can be strengthened via retrofitting projects in the pre-disaster stage to withstand the disaster [38, 56, 58]. The Transportation and Infrastructure Ministry of Türkiye (on August 26th, 2023) announced which highways would be reserved for FRs as part of preparation to better respond to a potential Istanbul earthquake and stated that critical structures on these roads would be strengthened. However, a detailed analysis regarding the urban roads has not been conducted.

The specific requirements of where people will be located at the time of the disaster, how many people will be mobile, and likewise, the number of immobile people to whom FRs should reach out, depends on the disaster. However, pre-disaster scenario analysis can provide insights into the impact of various choices of pre-selected FR paths. Every one of such scenarios is a complex mixed-integer non-linear program (MINLP) that is cumbersome to solve, in part because the objective function is itself an outcome of an optimization problem – that of selfish routing of evacuees using paths that are not allocated to a feasible set of FR paths – and not an algebraic function, and we aim to find the best set of FR paths incorporating evacuee behavior constrained by the FR path.

The primary methodological contribution of this paper is to explore a quantum-inspired approach to solving any one such deterministic instance of FRNDP. We anticipate this will be embedded in an outer loop that studies various scenarios, the parameters of each scenario having been

determined by experts in geology and practitioners of humanitarian operations. We hope our work adds to the optimization literature on (a) the disaster preparedness stage and is helpful towards such DM initiatives (not only in Türkiye that specifically motivated this research, but in other regions worldwide as well where such initiatives are being considered) and (b) the emerging area of quantum and quantum-inspired computing that appears promising to tackle complex MINLP models that capture the FRNDP and other complicated, yet critical real-world problems.

2 Related works

The *first responder network design problem* (FRNDP) is a variant of the discrete network design problem (DNDP), a well-studied bilevel optimization problem in transportation. The classic DNDP aims to identify an optimal set of candidate links to be adjusted in the network subject to a budget, taking into consideration users’ reactions to this alteration, typically governed by a traffic equilibrium perspective [10]. The DNDP can be expressed as a bilevel optimization problem, where the leader (outer) problem seeks to optimally determine a network design that minimizes a travel-oriented metric (e.g., total travel time) in the network, and the follower (inner) problem models the users’ reactions within the network [7]. This reaction is typically represented as a static traffic assignment problem (TAP), taking into account user equilibrium. The first exact method proposed to solve DNDP was a branch and bound method by [27], which used the system-optimum relaxation of the TAP, a convex programming problem, to generate lower bounds. A survey of exact methods to solve the DNDP is given by [40], where it is noted that the largest DNDP instances solved to optimality remain of small scale.

Three primary classes of methods have been proposed to solve the DNDP: a branch-and-bound algorithm [6, 15, 27, 55], a generalized Benders’ decomposition approach [6, 16–18] to solve a mixed-integer nonlinear programming formulation, and a single-level formulation created by using the (Karush–Kuhn–Tucker) KKT conditions since the TAP can be represented as a convex nonlinear program [7, 14, 16]. Several other papers solve the DNDP using techniques such as a linear approximation of the travel time function, system-optimum (SO) relaxations of their TAP models (a single-level optimization problem which ignores the follower objective function), and valid inequalities [31, 47, 48]. A hybrid machine learning and bi-objective optimization algorithm is proposed to solve a variant where lane closure and reversal decisions are made at the outer level to mitigate traffic congestion [57].

Several variants of DNDP have been proposed to establish emergency routes while considering the evacuation problem at the inner level [1, 37, 41]. [1] employed Benders Decomposition and heuristic accelerators as the solution approach. [37] identify the emergency transportation routes that will be closed to public traffic, as in our problem. Three objectives are optimized by a branch and cut algorithm. [41] also addresses a multi-objective disaster response routes design problem. However, multiple earthquake scenarios with the probability of failure of each arc are considered in a stochastic programming framework. A branch and cut algorithm is proposed to solve the nonlinear mixed integer program obtained by taking the weighted sum of the objectives. The need to reserve lanes for time-critical operations also arises during sports events such as the Olympics, where the athletes and equipment must travel between the venues within strict time windows. The problem of identifying which lanes to reserve to minimize the total weighted travel time increase for normal traffic while ensuring the time windows was defined as the lane reservation problem by [52]. Ignoring the inner traffic assignment problem in the DNDP, the authors provided a single-level mixed integer linear programming model and a greedy heuristic algorithm for its fast solution.

The FRNDP introduces additional layers of complexity compared to the classic DNDP. In the

DNDP, any feasible combination of arcs in the network can form a solution to the leader problem. However, the set of selected arcs for FR lane reservation in FRNDP must configure paths that connect the nodes requiring FR visits to one of the FR entry points in the network. Due to these constraints, it is not immediately clear how to extend the three methods mentioned above that solve the DNDP. Additionally, the conventional budget constraint significantly restricts the number of feasible solutions in DNDP. In contrast, FRNDP lacks this constraint, differentiating our problem from state-of-the-art variations of DNDP and expanding our search space into a combinatorially large realm.

Owing to its non-linear complex objective function subject to linear constraints, our study pioneers in investigating the application of a novel GAGA (GAMA + GAMA) algorithm in solving FRNDP instances. GAGA consists of a bi-level nested GAMA (Graver Augmented Multi-seed Algorithm). GAMA is a Quantum-Classical hybrid algorithm that consists of two main parts: finding the Graver basis and augmenting feasible solutions. GAMA finds successful applications in portfolio management [5, 46], cancer genomics [3], and Quadratic (Semi-) Assignment Problem [4].

3 First responder network design problem

We formally introduce the FRNDP as follows. The FRNDP is defined on a network with nodes N and directed links A . Let F be the set of nodes requiring an FR to visit them, and S be the set of nodes with disaster-affected individuals who aim to evacuate the network, referred to as *agents*. Moreover, let E be a set of critical nodes from where FRs can enter the network and agents can leave the network. Representing the travel demand right after the disaster, for each $i \in N$, let d_i be the number of agents (vehicles) at node i who evacuate the network. For each $(i, j) \in A$, let c_{ij} be the capacity of the link, T_{ij} be the free-flow travel time of the link, l_{ij} be the number of lanes on the link.

For each $(i, j) \in A$, let f_{ij} denote the number of agents traveling on link (i, j) . For each $(i, j) \in A$, let $t_{ij}(f_{ij})$ denote the travel time from node i to node j using link (i, j) , which depends on the flow along the link to account for traffic congestion. We assume that the travel time function is a strictly convex function and has the form $t_{ij}(f_{ij}) = T_{ij}(1 + \alpha(\frac{f_{ij}}{c_{ij}})^\beta)$, where we set $\alpha = 0.15$ and $\beta = 4$ following the Bureau of Public Roads (BPR) standard in [45]. We assume that agents decide to travel to an exit node in E , which can be altered depending on the behavior of other agents under optimal selfish routing behavior.

We must decide which lanes to *reserve* for FRs to use. We assume that reserving a lane means reserving one lane in both directions. This assumption is justified by the fact that many FRs will not only need to visit a node but also return to where they came from (and transport immobile people to exit points and so on). So, reserving a lane from a link (i, j) updates the capacities as follows: $c_{ij} \leftarrow \frac{l_{ij}-1}{l_{ij}}c_{ij}$ and $c_{ji} \leftarrow \frac{l_{ji}-1}{l_{ji}}c_{ji}$. Note that if more than one lane exists on a link, the unreserved lanes on this link can be used by mobile evacuees. We also assume that multiple nodes in F can use the same reserved lane to connect to their respective nodes in E without further affecting the capacity. The FRNDP seeks to find a set of lanes to reserve for FRs such that each node in F is connected to a node in E by these reserved lanes, and the sum of the exit times of overall evacuees located nodes in S at user equilibrium traffic is minimized.

3.1 Mixed integer non-linear programming (MINLP) model

We model the FRNDP as a mixed integer non-linear program as follows. We will define a bilevel program with outer problem P_o and inner problem P_i . The outer problem corresponds to choosing

which lanes to reserve for FRs, and the inner problem corresponds to solving the user equilibrium traffic problem (with $\delta_{ik} = 1$ if $i = k$ and zero otherwise).

$$(P_o) \quad \min_y \sum_{(i,j) \in A} x_{ij} t_{ij}(x_{ij}, y_{ij}, y_{ji}) \quad (1)$$

$$\text{s.t.} \quad \sum_{j \in N: (i,j) \in A} y_{ijk} - \sum_{j \in N: (j,i) \in A} y_{jik} = \delta_{ik} \quad \forall i \in N \setminus E, \forall k \in F \quad (2)$$

$$y_{ijk} \leq y_{ij} \quad \forall (i,j) \in A, \forall k \in F \quad (3)$$

$$y_{ij} \in \{0, 1\} \quad \forall (i,j) \in A \quad (4)$$

$$y_{ijk} \in \{0, 1\} \quad \forall (i,j) \in A, \forall k \in F \quad (5)$$

$$x \in \mathcal{S}_y^* \quad (6)$$

$$(P_i) \quad \min_x \sum_{(i,j) \in A} \int_0^{x_{ij}} t_{ij}(v, y_{ij}, y_{ji}) dv \quad (7)$$

$$\text{s.t.} \quad \sum_{j \in N: (i,j) \in A} x_{ij} - \sum_{j \in N: (j,i) \in A} x_{ji} = d_i \quad \forall i \in N \setminus E \quad (8)$$

$$x_{ij} \geq 0 \quad \forall (i,j) \in A \quad (9)$$

The outer problem P_o is defined as follows. For each link $(i, j) \in A$, we define a binary variable y_{ij} that represents the choice of reserving a lane for FRs. For each link $(i, j) \in A$ and each node $k \in F$, we define a binary variable y_{ijk} that represents the choice of an FR using the link to reach node k . This second set of binary variables will be useful because of the assumption that multiple nodes in F can be connected to a node in E using the same reserved link. The objective function (1) is to minimize the sum of the total travel times of all agents from their initial nodes to an exit. We rewrite the time travel function for a given link $(i, j) \in A$ as $t_{ij}(f_{ij}, y_{ij}, y_{ji}) = T_{ij}(1 + \alpha(\frac{f_{ij}}{c_{ij}(y_{ij}, y_{ji})})^\beta)$ to explicitly express that the functions c_{ij} and t_{ij} depend on variables y_{ij} and y_{ji} . Constraints (2) ensure that each node in F is connected by reserved lanes to an FR entry node. Constraints (3) ensure that a lane from the link (i, j) is considered reserved if one or more nodes in F use the link to connect to an FR entry node. Constraints (4 and 5) require the y variables to be binary. Constraint (6) ensures that the solution to P_o uses an optimal solution to P_i , where x is the set of inner problem variables and P_i^* is the set of optimal solutions to P_i for a solution y .

Next, we describe the inner problem P_i . The model is based on a given feasible solution y to the outer problem P_o . For each link $(i, j) \in A$, we define a continuous variable x_{ij} that represents the flow of agents evacuating the network using the link. The objective (7) is the standard objective function used in selfish routing problems ([8]), albeit with the updated travel time function that indicates how link capacities may be updated due to reserved lanes. Constraints (8) ensure that all agents at nodes in S reach an exit node E . Constraints (9) enforce the non-negativity of the x variables. We assume that allowing a fractional number of agents gives a close enough approximation to enforcing the more realistic requirement that the flow along each link must be an integer number of agents.

4 Quantum-inspired algorithm

In this section, we develop a bi-level optimization algorithm for the FRNDP, building on the Graver Augmented Multi-seed Algorithm (GAMA) developed in [5] and [4]. First, we outline the GAMA algorithm below for the sake of completeness.

4.1 GAMA

GAMA is a heuristic algorithm for solving general non-linear integer optimization problems of the form

$$(\mathcal{IP})_{A,b,l,u,f} = \begin{cases} \min f(x) \\ Ax = b & l \leq x \leq n \quad x, l, u \in \mathbb{Z}^n, \\ A \in \mathbb{Z}^{m \times n} \quad b \in \mathbb{Z}^n \end{cases} \quad (10)$$

where $f : \mathbb{R}^n \rightarrow \mathbb{R}$ is a real valued function. One approach to solving such problems is to use an augmentation procedure. An augmentation procedure starts from an initial feasible solution and, at each iteration, checks for an improvement step by using directions from a set of candidate improvement directions, referred to as a test set or optimality certificate. When none of the candidate directions can yield an improvement step, the algorithm terminates. We define the test set below (definition taken verbatim from [5]).

Definition 1 *A set $S \in \mathbb{Z}^n$ is a test set or an optimality certificate if for every non-optimal, feasible solution, x_0 , there exists $t \in S$ and $\lambda \in \mathbb{Z}_+$ such that $f(x_0 + \lambda t) < f(x_0)$. The vector t is called the augmenting direction.*

The GAMA algorithm uses a Graver basis [21] as a test set. We provide a definition of the Graver basis below (taken verbatim from [5]). To understand the definition of Graver basis, we first give two auxiliary definitions.

Definition 2 *Given $x, y \in \mathbb{R}^n$, we define x is conformal to y , written as $x \sqsubseteq y$, if $x_i y_i \geq 0$ (x and y lie in the same orthant), and $|x_i| \leq |y_i|$, $\forall i \in \{1..n\}$. A sum $u = \sum_i v_i$ is called conformal if $v_i \sqsubseteq u$, $\forall i$.*

For a matrix $A \in \mathbb{Z}^{m \times n}$, define the lattice

$$L^*(A) = \{x | Ax = 0, x \in \mathbb{Z}^n, A \in \mathbb{Z}^{m \times n}\} \setminus \{0\}. \quad (11)$$

Definition 3 *The Graver basis, $\mathcal{G}(A) \subset \mathbb{Z}^n$, of an integer matrix A is defined as the finite set of \sqsubseteq minimal elements in $L^*(A)$ (i.e., $\forall g_i, g_j \in \mathcal{G}(A)$, $g_i \not\sqsubseteq g_j$, when $i \neq j$).*

The Graver basis [21] of an integer matrix $A \in \mathbb{Z}^{m \times n}$ is known to be a test set for integer linear programs. Graver basis is also a test set for certain non-linear objective functions, including Separable convex minimization [36], Convex integer maximization [11], Norm p minimization [23], Quadratic [29, 36] and Polynomial minimization [29]. It has also been shown that for these problem classes, the number of augmentation steps needed is polynomial [11, 23]. Graver basis can be computed (only for small size problems) using classical methods such as the algorithms developed by [39] and [42].

For general non-linear, non-convex optimization problems such as the \mathcal{IP} defined in 10, it is not known if the Graver basis is a test set. However, if a non-convex objective function can be viewed as many convex functions stitched together, then the entire feasible solution can be viewed

as a collection of parallel subspaces with convex objective functions. Given the Graver basis for the constraint matrix and feasible solutions in each of these subspaces, we can find a global optimal by augmenting along the Graver basis from each of the feasible solutions to reach a local optimal solution and find the best possible solutions among the local optima.

In case we are unsure whether the Graver basis serves as a test set or encounters computational challenges, a pragmatic approach involves leveraging GAMA as a heuristic, utilizing a *partial Graver basis*. A partial Graver basis is a subset of the Graver basis. Using a partial Graver basis, GAMA gives a feasible but not provably optimal solution. Such a method has been studied in [4, 5], where the heuristic is improved by starting GAMA from multiple initial feasible solutions to the constraint equations as starting points (seeds) instead of just one.

4.2 Partial Graver basis computation

In general, a partial Graver basis can be obtained as follows. The method finds points in $L^*(A)$ by taking the differences of feasible solutions. Then, a classical post-processing step by \sqsubseteq -minimal filtering [4] yields a partial Graver basis.

To obtain a sample of feasible solutions to \mathcal{IP} , so that we can take their differences, we solve a quadratic unconstrained integer optimization (QUIO) given by

$$\begin{aligned} \min \quad & x^T Q_I x - 2b^T A x \\ & Q_I = A^T A, x \in \mathbb{Z}^n. \end{aligned} \tag{12}$$

If the variable x is an integer, a binary encoding of the integer variables is required. Expressing

$$x = L + EX, \tag{13}$$

with L as the lower bound vector and E as the encoding matrix, we get a Quadratic Unconstrained Boolean Optimization (QUBO)

$$\begin{aligned} \min \quad & X^T Q_B X \\ & X \in \{0, 1\}^{nk}, \end{aligned} \tag{14}$$

where $Q_B = E^T Q_I E + 2\text{diag}[(L^T Q_I - b^T A)E]$ and $Q_I = A^T A$.

The above QUBO can be solved via an annealer or by means of simulated annealing [26] to obtain a sample of feasible solutions. An annealer refers to a specially constructed quantum or semi-classical hardware [9, 19, 22, 25, 32, 33, 35, 49, 50] used for solving QUBO problems mapped to an Ising model.

4.3 GAMA for FRNDP

We now explain how GAMA attempts to solve FRNDP by only searching on FR paths. The inner problem is solved using a gradient descent algorithm from [28].

For each node $k \in F$, we obtain a sample of n_{paths} feasible paths, each of which is connected to some FR entry node in E . These feasible paths are obtained by solving a QUBO (implied by equations 2) using a quantum annealing device (such as D-Wave), classical simulated annealing, or by using a path-finding algorithm such as Yen's algorithm for k-shortest paths [54]. We create feasible solutions for the entire network by combining the feasible FR paths for each point in F . (This gives us M seeds.)

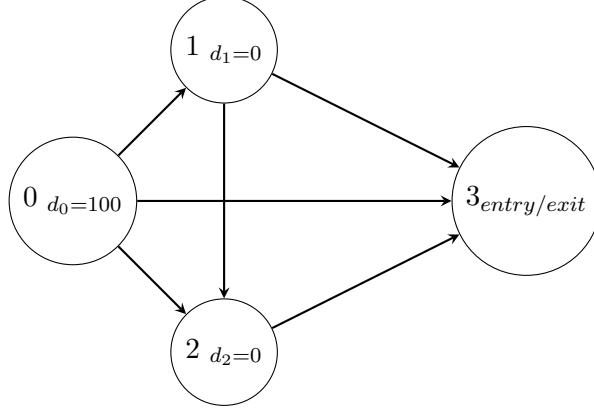


Figure 1: An example of a 4-node network.

A set of lattice elements (recall equation 11) can be obtained by taking differences of these feasible solutions. Then, a partial Graver basis is obtained from these lattice elements using the procedure in [4, 5] that ensures that all elements are conformal minimal.

As in [4, 5], we start the augmentation algorithm from M initial feasible solutions. Rather than take all feasible solutions as seeds, we construct a random sample of M feasible solutions by combining randomly chosen paths for each $k \in F$ from the corresponding set of n_{paths} paths that we obtained when calculating the partial Graver basis. So, for each initial feasible solution, we randomly select a path for each $k \in F$, and combine the paths to obtain a feasible solution of y_{ijk} variables. An assignment of the y_{ij} variables follows naturally.

Using a partial Graver basis and M initial seeds, GAMA works as follows. For each initial seed, start from the corresponding initial feasible solution. Then, check each direction in the partial Graver basis to update the variables y_{ijk} and y_{ij} . To check a direction, use step size $t = 1$ and run the gradient descent algorithm from [28] to calculate the values of the x variables. If a step is improving, the solution is updated along the step and the directions in the Graver basis are checked again. The algorithm terminates when no step gives an improved objective function value from the current one.

We illustrate GAMA using an example.

4.3.1 Example with a 4-Node Network

Consider a 4-node network graph, $G = (N, A)$ with $N = \{0, 1, 2, 3\}$ and $A = \{(0, 1), (0, 2), (0, 3), (1, 2), (1, 3), (2, 3)\}$ with one lane in each edge. If a FR lane is allocated to an edge, no demand can flow through it in the opposite direction. For simplicity, we will also assume a single entry/exit: node 3. The demand is also present at a single location: node 0. So, we have set of nodes requiring FR, $F = \{0\}$ and critical nodes, $E = \{3\}$ and agent node, $S = \{0\}$. Let $d_0 = 100$. The arrows in the graph show the evacuee direction via different edges, if available, from node 0 to node 3. Recall that there is only one lane for each edge. Therefore, assigning an FR path to an edge makes it unavailable for evacuating. The capacities on the edges are $C = \{25, 30, 35, 35, 15, 45\}$, and the free flow travel time is taken as 1.

We suppress the index $k = 0$ here as it is the only demand node. With $y = (y_{01}, y_{02}, y_{03}, y_{12}, y_{13}, y_{23})$, the FR path constraints are

$$y_{01} + y_{02} + y_{03} = 1 \quad (15)$$

$$y_{12} + y_{13} - y_{01} = 0 \quad (16)$$

$$y_{23} - y_{02} - y_{12} = 0 \quad (17)$$

where $y_{ij} \in \{0, 1\}$.

The above constraints can be expressed as $A_{FR}X_{FR} = B_{FR}$ with

$$X_{FR} = \begin{pmatrix} y_{01} \\ y_{02} \\ y_{03} \\ y_{12} \\ y_{13} \\ y_{23} \end{pmatrix}, A_{FR} = \begin{pmatrix} 1 & 1 & 1 & 0 & 0 & 0 \\ -1 & 0 & 0 & 1 & 1 & 0 \\ 0 & -1 & 0 & -1 & 0 & 0 \end{pmatrix}, B_{FR} = \begin{pmatrix} 1 \\ 0 \\ 0 \end{pmatrix}.$$

There are a total of 4 feasible solutions given by

$$Y_{FR,feasible} = \begin{pmatrix} 1 \\ 0 \\ 0 \\ 1 \\ 0 \\ 1 \end{pmatrix}, \begin{pmatrix} 1 \\ 0 \\ 0 \\ 0 \\ 1 \\ 0 \end{pmatrix}, \begin{pmatrix} 0 \\ 1 \\ 0 \\ 0 \\ 0 \\ 1 \end{pmatrix}, \begin{pmatrix} 0 \\ 0 \\ 1 \\ 0 \\ 0 \\ 1 \end{pmatrix}.$$

The lattice elements satisfying $A_{FR}X_{FR} = 0$ can be obtained as a difference of the feasible solutions given by

$$Y_{FR,kernel} = \begin{pmatrix} 0 \\ 0 \\ 0 \\ 1 \\ -1 \\ 1 \end{pmatrix}, \begin{pmatrix} 1 \\ -1 \\ 0 \\ 1 \\ 0 \\ 0 \end{pmatrix}, \begin{pmatrix} 1 \\ 0 \\ -1 \\ 1 \\ 0 \\ 1 \end{pmatrix}, \begin{pmatrix} 1 \\ -1 \\ 0 \\ 0 \\ 1 \\ -1 \end{pmatrix}, \begin{pmatrix} 1 \\ 0 \\ -1 \\ 0 \\ 1 \\ 0 \end{pmatrix}, \begin{pmatrix} 0 \\ 1 \\ -1 \\ 0 \\ 0 \\ 1 \end{pmatrix}.$$

The lattice elements are already conformally minimal elements and so form a subset of the full Graver basis. So, the lattice elements $Y_{FR,kernel}$ is a partial Graver basis set in this instance. The full Graver basis (obtained using Pottier's algorithm [39]) is given by

$$\mathcal{G}(A_{FR}) = \begin{pmatrix} 1 & 1 & 0 & -1 & -1 & 0 & 1 & -1 & 0 & 0 & 1 & -1 & 0 & 0 \\ -1 & 0 & 1 & 1 & 0 & -1 & 0 & 0 & -1 & 1 & -1 & 1 & 0 & 0 \\ 0 & -1 & -1 & 0 & 1 & 1 & -1 & 1 & 1 & -1 & 0 & 0 & 0 & 0 \\ 1 & 0 & 0 & -1 & 0 & 0 & 1 & -1 & 1 & -1 & 0 & 0 & 1 & -1 \\ 0 & 1 & 0 & 0 & -1 & 0 & 0 & 0 & -1 & 1 & 1 & -1 & -1 & 1 \\ 0 & 0 & 1 & 0 & 0 & -1 & 1 & -1 & 0 & 0 & -1 & 1 & 1 & -1 \end{pmatrix}.$$

Given how small the example is, we can enumerate all FR path choices and compute the resulting total evacuation time in equilibrium given that FR choice. See Table 1. Note the almost identical travel time for each evacuation path under user equilibrium at each FR choice. We can see that FR Path - 2 is optimal for the objective of total time for evacuation.

Now, we will illustrate steps in GAMA. Suppose we use only one of the feasible FR solution as a seed (M=1), namely (3,0) with ID-1 in Table 1. The solution is $X_{FR} = (0 \ 0 \ 1 \ 0 \ 0 \ 0)^T$. We

ID	FR-Path	Evac. paths	Path evac. time	Total evac. time
1	(3, 0)	$P_1 : (0, 1, 3)$ $P_2 : (0, 1, 2, 3)$ $P_3 : (0, 2, 3)$	5.02 5.18 5.08	507.56
2	(3, 1, 0)	$P_1 : (0, 2, 3)$ $P_2 : (0, 3)$	2.51 2.38	243.43
3	(3, 2, 0)	$P_1 : (0, 1, 3)$ $P_2 : (0, 3)$	4.06 3.67	379.01
4	(3, 2, 1, 0)	$P_1 : (0, 3)$	11.00	1099.58

Table 1: Agent evacuation times for each FR in a 4-node example.

solve the inner problem, \mathcal{P}_i to obtain the optimal user equilibrium objective. The optimal flow values are found to be $X_{FL}^* = (42 \ 58 \ 0 \ 14 \ 28 \ 72)^T$. Using these flow values on the edges, we evaluate the total evacuation time, which is $T = 507.56$. Note that the travel time along the 3 possible evacuation routes, P_1, P_2, P_3 are approximately similar. They are not the same because of integrality constraints.

Now, we start the Graver augmentation. Consider the direction with Graver element, $g_0 = (1 \ -1 \ 0 \ 1 \ 0 \ 0)^T$. Clearly, $X_{FR}^0 + g_0$ is infeasible. Consider the next Graver element, $g_1 = (1 \ 0 \ -1 \ 0 \ 1 \ 0)^T$. Here $X_{FR}^1 = X_{FR}^0 + g_1 = (1 \ 0 \ 0 \ 0 \ 1 \ 0)^T$ which is the FR-path with ID-2. Solving the inner problem in this case gives the optimal flow values, $X_{FL}^* = (0 \ 39 \ 61 \ 0 \ 0 \ 39)^T$ with a total evacuation time of $T = 243.43$. This is better than $T = 507.56$. So, we update the optimal FR path to X_{FR}^1 .

Continuing with the Graver walk, the next feasible solution is $X_{FR}^1 + g_4$, with $g_4 = (-1 \ 0 \ 1 \ 0 \ -1 \ 0)^T$ which is again X_{FR}^0 . Since the evacuation time is not improved, the FR path remains current at X_{FR}^1 . The next feasible FR path in the course of the Graver walk is $X_{FR}^3 = X_{FR}^2 + g_{11}$ with $g_{11} = (-1 \ 1 \ 0 \ 0 \ -1 \ 1)^T$ and $X_{FR}^3 = (0 \ 1 \ 0 \ 0 \ 0 \ 1)^T$, $X_{FL}^* = (35 \ 0 \ 65 \ 0 \ 35 \ 0)^T$ with evacuation time of 379.01 and then $X_{FR}^4 = (1 \ 0 \ 0 \ 1 \ 0 \ 1)^T$, $X_{FL}^* = (0 \ 0 \ 100 \ 0 \ 0 \ 0)^T$ using the Graver element, $g_{12} = (0 \ 0 \ 0 \ 1 \ -1 \ 1)^T$ with evacuation time of 1099.58. At this point, we have verified that no further augmentation is possible from X_{FR}^2 and the algorithm terminates with X_{FR}^2 as the optimal FR path solution.

4.4 GAGA: Bi-level nested GAMA within GAMA

A further methodological enhancement of this work is to attempt to solve the inner optimization with GAMA itself. The motivation is that approximately solving P_i at each step will accelerate the search, because exactly solving P_i has been difficult. The solution to P_i that GAMA finds, however, is an approximation because GAMA uses a partial Graver basis for its search. However, upon termination, our procedure will add another step: solve P_i using the exact solution method by [28]. To the best of our knowledge, this is the first time that a heuristic like this has been studied. We call this algorithm that is GAMA within GAMA as GAGA.

We construct each initial feasible solution as follows. For each node $k \in S$, we randomly and independently sample d_k paths from the set of n_{paths} paths and send one evacuee along each path. As before, to generate a partial Graver basis with respect to the constraint matrix in P_i , we find lattice elements that are differences of paths between nodes with evacuees in S and exit nodes in E , and then apply the same procedure to end up with conformally minimal solutions. To create many of these paths, for each node, $k \in S$, we generate a sample of n_{paths} feasible paths to exit nodes in E . As before, this can be done with an annealer, simulated annealing, or a path-finding algorithm.

The inner GAMA solves P_i as follows. We start from each of the M different initial solutions. At each step, the algorithm checks each possible improving direction in the Graver basis, using a step size of $t = 1$, and updates the current solution as soon as an objective improving direction is found. We terminate the inner GAMA when there is no improving direction up to a tolerance. Without a tolerance threshold, the Graver augmentation runs until there is no improving direction amongst all the Graver basis elements. A tolerance threshold ensures that the run is assumed to be completed if the change in the objective function after one complete pass over all the Graver basis elements is below the tolerance threshold. We experiment with and without a tolerance threshold of 10^{-3} for the inner problem.

We note that the Graver augmentation for P_i is carried out using both a partial Graver basis and integral flow values. Hence, it is possible and can be expected that the user equilibrium flow obtained by the GAMA heuristic is a close approximation to, but not the exact user equilibrium flow solution. Therefore, as a final step, we run the gradient descent algorithm from [28] on each of the local optimal FR solutions at the end of the GAMA and report the optimal total evacuation time under this user flow equilibrium as the optimized result. In the rest of the paper, we denote the final solution obtained at the end of the GAMA procedure as *GAGA-only* and the solution after running the additional step of the gradient descent method from [28] as *GAGA-LeBlanc*. Unless explicitly stated otherwise, the final solutions presented refer to the *GAGA-LeBlanc* values.

To summarize, the GAGA algorithm works as follows. We run the (outer) GAMA heuristic to solve P_o and at each step we solve P_i using (inner) GAMA up to a tolerance. In order to speed up the computation, we use the current equilibrium flow solution as the initial feasible solution to the inner problem. The GAGA algorithm terminates when none of the directions in the partial Graver basis (outer and inner) can improve the current solution.

5 Branch-and-Bound algorithm

We develop a branch-and-bound algorithm to solve the FRNDP to evaluate the performance of GAGA. The method is based on an algorithm that was first developed by [27] and later extended in [15] by solving the system optimal relaxation of the DNDP—instead of the traffic assignment problem. The algorithm is adapted to consider the additional constraints of the FRNDP regarding reserving links for first responders. Next, we will describe the details of the branch-and-bound algorithm, including the primal heuristic, branching rule, dual-bound heuristic, and node selection heuristic. We recognize that more sophisticated heuristics can be developed and tested. Still, we believe that this version of the branch-and-bound algorithm which is considered among the most efficient exact solution methodologies in the literature [40] provides a worthy comparison for GAGA.

We use the following primal heuristic to find a feasible solution to P_o . First, we compute the shortest path from each node in E to each node in F using Dijkstra’s algorithm. Then, for each node in F , we reserve the links along the shortest of these paths, which corresponds to an assignment of the variables y . Next, we solve P_i by using a gradient descent algorithm from [28]. This gradient descent algorithm solves each subproblem by several shortest path calculations for each node in S . The algorithm uses a halving method to calculate the step size, and we use a relative tolerance of 0.001 to determine when to terminate gradient descent, which we denote as ϵ . We use a greedy heuristic at the root node to find an initial feasible solution to begin the gradient descent algorithm. At a node that is not the root node, to accelerate the gradient descent algorithm, we initialize a feasible solution with the optimal solution of the parent node.

Next, we describe the branching rule. We develop a branching procedure that creates two child nodes in the branch-and-bound tree based on a given link: one that requires a solution to reserve

this link and one that requires a solution not to reserve this link. So, we develop a method of choosing the particular link to use in the branching procedure at a given node. We maintain an order of the nodes in F , so given the link that created the branch for the current node based on some $i \in F$, we consider the next node $j \in F$ based on the order. Given this node, based on the solution y , we order the links that connect j to an exit node $k \in E$, starting from the exit node. We select the first link that has not yet been fixed to be used or not used at the current node.

We can calculate a dual bound by solving for the total evacuation time of a *system optimal* (i.e., authoritarian) solution. We solve this problem by using the same gradient descent algorithm as the one described above. Similar to previous literature, we notice that the lower bounds are not effective in fathoming search nodes in the branch-and-bound tree. Thus, to improve the algorithm’s efficiency, we forego calculating lower bounds in our experiments. It would likely be useful to implement lower-bound computations similar to the ones done in [15]. As a consequence of not calculating lower bounds, we implement a breadth-first node selection heuristic instead of another commonly used heuristic that chooses the next node to solve based on lower bounds.

6 Experimental results

We evaluate the performance of GAGA on two types of instances: random instances and instances created with data from Istanbul, Türkiye, which is under serious earthquake risk. As pointed out in recent news [12], Istanbul is expected to be hit by an earthquake with a magnitude above 7.0 in the upcoming seven years at a probability of 64 percent. Therefore, the problem we solve carries great significance for the preparedness of Istanbul.

In our experiments, we compare the performance of GAGA to that of the branch-and-bound method, which we will refer to as BB. Throughout the experiments, we vary the following parameters of GAGA.

- The number of reads or samples in the simulated annealing step or using a D-Wave annealer. We denote this value as $n_{samples}$ and compare $n_{samples} = 10000$ and with $n_{samples} = 1000$.
- The number of paths from/to each node $i \in N \setminus E$. We set $n_{paths} = 25$ as a default and experiment with other values of n_{paths} for a single instance.

6.1 Random graph instances

We create the first set of instances by constructing small random graphs and randomly generating the other relevant data. These graphs serve as an initial evaluation of GAGA’s performance and a comparison of its performance with that of BB.

6.1.1 Instance generation

We create randomly generated instances as follows. We start with input parameters for the number of nodes n and the probability of an edge being between two nodes p . We produce n nodes on a two-dimensional grid, randomly generating each coordinate from a uniform $[0,1]$ distribution. Then, we produce $\frac{n}{10}$ nodes as exits nodes E on the boundary of the unit square. Then, for each pair of nodes, we create edges in the graph with a probability that is the product of p and an additional factor based on the distance between the two nodes. The capacities of each edge are generated from a normal distribution with an average of 50 and a standard deviation of 20. We assign each edge to have two lanes in both directions. We create the demands d at each node from a normal distribution with mean 100 and standard deviation 10. We generate ten instances of each

type and denote the instance number by i . If an instance solution is found to be infeasible, we create another instance until we have ten instances with feasible solutions. The random instances are generated with the number of nodes $n = 10, 20, 30$, each with $p = 0.5$ and $p = 0.75$.

6.2 Details of processor used for computational experiments

The GAGA is implemented on a single core of Intel Xeon Gold 6252 @ 2.10 GHz (Processor-G) with 192GB memory and 48 cores. The Branch and bound have been carried out on a single core of Intel(R) Xeon(R) Gold 6248R CPU @ 3.00GHz (Processor-B) with 64 GB memory and 8 cores. Based on a benchmarking comparison in *PassMark*, the single-core performance of Processor-B is found to be better. Since no numerical factor is provided there, we compared the run times between the two processors for the $n = 30, p = 0.75$ case. We found (see Appendix A) that Processor-B is faster in all the 10 random instances and by a factor of ~ 1.3 on average. Regardless, when we report the times, we have not scaled it by any factor.¹

6.2.1 Testing the performance of D-Wave

Using random graphs, we test the applicability and performance of the D-Wave² quantum annealing device in generating a sample of feasible solutions required for the GAGA algorithm. We generate the feasible solutions for $n = 10$ random instances with $p = 0.5, 0.75$. The experiments have been performed on the D-Wave Advantage-system4.1 machine with an annealing time of $1\mu s$ and 1000 samples. Following the annealing schedule, a post-processing step using a steepest descent solver from D-Wave Ocean tools is carried out. This step is found to be necessary to obtain a larger sample of feasible solutions. The feasible solutions to the constraint equations in Equations (2), (8) generate a set of feasible paths from a given node, $i \in N \setminus E$ to one of the critical nodes, E . However, the constraints, as shown in Equations (2), (8), also allow cyclic paths as part of the solutions. We run a Dijkstra algorithm starting from the demand node, $k \in N \setminus E$, to one of the exit nodes, using only the arcs with $y_{ijk} = 1$ in the feasible solution. For dense graphs, we found that the cyclic paths are obtained at the nodes present along the path from the node $k \in N \setminus E$ to one of the exits in E . This can be eliminated by adding the following additional constraint system to the QUBO, requiring that there is only a maximum of one outward edge at each node.

$$\sum_{j \in N: (i,j) \in A} y_{ijk} + a_{ik} = 1, \forall i \in N \setminus E \quad (18)$$

where $a_{ik} \in \{0, 1\}$ is an auxiliary variable for a given node k , from which a feasible path to the critical nodes E is needed.

After generating the feasible solutions and post-processing, we compute the partial Graver basis and carry out a Graver augmentation, followed by a final [28] algorithm call, as alluded to in Section 4.4. We similarly generate feasible solutions using simulated annealing. We use the D-Wave Ocean tools' classical Neal sampler for carrying out the simulated annealing with 1000 and 10000 samples. The results are then compared with the Branch-and-Bound (BB) algorithm. We tabulate the results along with the total computational time in Table 2. The BB algorithm is given a time of 600 seconds for this instance as the total time with the GAGA algorithm in all the cases is below this time. As seen from the table, the GAGA solutions obtained using D-Wave solutions

¹We further note that only a single core is used for the computational experiments in both the GAGA and Branch-and-Bound runs. There is no parallel processing involved, although there appears good possibility of developing such algorithms. So, the different number of cores in the two processors is not relevant for the comparison of run times.

²<https://www.dwavesys.com/>

(DWaveAdv4.1-1000) and the simulated annealing solutions with $n_{samples} = 1000, 10000$ reads (GAGA-SA-1000, GAGA-SA-10000) are comparable for both $p = 0.5$ and $p = 0.75$. Compared with Branch-and-Bound (BB), it can be seen that GAGA results are similar for $p = 0.5$ and are relatively better at $p = 0.75$.

The D-Wave annealer generates feasible solutions only for the graphs of node size $n = 10$. We tested the D-Wave annealer using one instance of a graph with $n = 20$ nodes ($p = 0.5, i = 0$) with both the Advantage-System 4.1 and Advantage-System 6.3 machines using $n = 1000$ samples. However, we cannot generate feasible solutions for all the demand nodes. Hence, we only present results with feasible solutions generated using simulated annealing in the rest of the paper.

Instance			GAGA-SA-1000		DWaveAdv4.1-1000		GAGA-SA-10000		Branch-And-Bound	
n	p	i	obj	time (s)	obj	time (s)	obj	time (s)	obj	time (s)
10	0.5	0	6.59 e+07	19.81	6.42 e+07	21.33	6.65 e+07	86.70	6.60 e+07	600
10	0.5	1	8.08 e+06	161.53	8.49 e+06	118.71	8.18 e+06	251.63	8.16 e+06	600
10	0.5	2	1.27 e+08	45.98	1.26 e+08	43.37	1.26 e+08	123.12	1.27 e+08	600
10	0.5	3	11.52 e+08	33.43	4.15 e+08	33.50	4.15 e+08	101.85	4.16 e+08	600
10	0.5	4	5.52 e+07	94.43	5.53 e+07	73.67	5.53 e+07	176.50	5.53 e+07	600
10	0.5	5	2.20 e+08	140.90	2.24 e+08	123.16	2.21 e+08	234.15	2.21 e+08	600
10	0.5	6	6.67 e+06	150.72	8.06 e+06	162.21	6.93 e+06	247.18	6.80 e+06	600
10	0.5	7	9.12 e+07	51.76	1.23 e+07	52.02	2.60 e+07	115.27	6.81 e+07	600
10	0.5	8	4.24 e+06	48.42	4.08 e+06	47.21	4.44 e+06	125.42	4.13 e+06	600
10	0.5	9	6.79 e+07	177.53	7.85 e+07	138.79	6.78 e+07	276.38	1.01 e+08	600
10	0.75	0	1.99 e+05	241.60	2.08 e+05	241.32	1.97 e+05	413.56	2.29 e+05	600
10	0.75	1	5.06 e+05	276.44	5.54 e+05	239.37	4.96 e+05	405.03	6.27 e+05	600
10	0.75	2	4.84 e+06	182.41	5.36 e+06	172.65	4.85 e+06	285.60	6.89 e+06	600
10	0.75	3	3.05 e+05	258.83	3.10 e+05	188.40	2.91 e+05	453.60	3.32 e+05	600
10	0.75	4	1.88 e+06	290.05	1.74 e+06	239.80	1.86 e+06	445.27	1.98 e+06	600
10	0.75	5	3.78 e+05	233.02	3.76 e+05	145.28	3.82 e+05	433.21	5.81 e+05	600
10	0.75	6	1.81 e+05	227.59	1.92 e+05	248.97	1.81 e+05	418.50	2.14 e+05	600
10	0.75	7	7.70 e+04	263.95	7.20 e+04	263.13	7.70 e+04	452.06	7.67 e+04	600
10	0.75	8	2.69 e+06	292.89	2.69 e+06	354.23	2.69 e+06	446.26	5.07 e+06	600
10	0.75	9	1.61 e+05	316.29	1.71 e+05	214.42	1.61 e+05	496.67	1.74 e+05	600

Table 2: Results comparing D-Wave Advantage 4.1 output using 1000 samples (with an anneal time of $1\mu s$ per sample) and simulated annealing using 1000, 10000 samples on random instances with $n=10$ nodes randomly generated in $U(0,1)$, p probability of an edge with an additional factor based on distance, i instance number. An additional $\frac{n}{10}$ nodes are marked as exits on the boundary of the unit square. These also serve as FR entry points. Capacities of edges are $N(50,20)$. All edges have 2 lanes in both directions. The population at each node to exit is $N(100,10)$. For each instance, the entry for the method with the best performance is in bold text.

6.2.2 Path generation methods

In Table 3, we compare the GAGA algorithm implemented using feasible solutions generated with simulated annealing and the Branch-and-Bound results. Additionally, we generate a set of feasible solutions using the Yen’s k -shortest path algorithm as an alternative to simulated annealing. In all these instances, the BB algorithm is given a run time of 14000s, which is longer than the maximum time taken for the GAGA run on any of these instances. The simulated annealing runs are carried out with $n_{samples} = 1000$ and 10000 to test the dependence of the quality of the solution on the $n_{samples}$ parameter. We refer to these as GAGA-SA-1000 and GAGA-SA-10000, respectively. The results using feasible solutions from Yen’s algorithm are referred to as GAGA-Yens. From the

table, we can see that the solutions are comparable among GAGA-SA-1000, GAGA-SA-10000, as well as GAGA-Yens. Compared with Branch-and-Bound, we can see that the results from the GAGA algorithm have a better solution quality. We observed here (not shown in any table for space reasons) that using $n_{samples} = 10000$, the solution obtained with the GAGA algorithm before the [28] algorithm call (i.e., GAGA-*only* results) is better than the solutions for the same obtained using $n_{samples} = 1000$ or the Yen’s algorithm. We attribute this to a lack of diversity on the partial Graver basis. We explore this in detail for a single instance in the subsection below.

6.2.3 Varying the parameter n_{paths}

To understand the impact of increasing the number of Graver elements, we examine a single random instance ($n = 30$, $p = 0.75$, $i = 1$) in further detail. This instance is chosen because the solution from GAGA-Yen’s algorithm is slightly higher when compared to the GAGA-SA-10000 result. In particular, we explore the effect of changing n_{paths} and compare GAGA-SA-10000 and GAGA-Yens results. We vary the n_{paths} from 20 to 40 in steps of 5. We show the solution and time to solution in Table 4. The solution at the end of the GAGA run (GAGA-*only*) is shown in brackets. The table shows that the GAGA-*only* result is comparable with the GAGA-*LeBlanc* for the GAGA-SA-10000. The effects of changing n_{paths} are negligible. On the other hand, if we examine the GAGA-Yens results, we can see that the GAGA-*only* results are significantly larger than the GAGA-*LeBlanc* values. While the effect of n_{paths} is not significant on the final solution, we can see that the GAGA-*only* solution decreases with increasing n_{paths} (which also leads to an increase in the number of Graver elements, which we denote as n_{graver}).

6.2.4 Experimenting with interchanging initial seeds and Graver basis from different path generation methods

To further understand the effects of the initial seeds and partial Graver basis elements, we run the GAGA algorithm using initial seeds generated from GAGA-SA-10000/GAGA-Yens and the partial Graver basis from GAGA-Yens/GAGA-SA-10000. The results are compared in Table 5. The final GAGA-*LeBlanc* values are comparable in all cases. Instead, if we compare the GAGA-*only* solutions, we can see that the best result is obtained when using GAGA-SA-10000 solutions both for generating the initial solutions and the Graver elements. If we use initial seeds from GAGA-SA-10000 solutions but generate the Graver basis elements using GAGA-Yens, the GAGA-*only* results are worse by 2 orders of magnitude. This can be attributed to the Graver basis elements from GAGA-Yens not being able to cover the domain of the paths found in the GAGA-SA-10000 initial feasible solutions.

Given that the quality of solutions is consistently better with the GAGA-SA-10000 feasible solutions in $n = 30$ and $p = 0.75$ experiments, and we had observed that GAGA-*only* solutions are better for $n = 10000$ (versus $n = 1000$ for SA), in Section 6.3, we decided to use feasible paths generated by simulated annealing run with $n_{samples} = 10000$.

6.3 Case study: Istanbul instances

We generate three sample instances based on the city of Istanbul, Türkiye. This enables us to assess GAGA’s performance on a real-life urban road network. The case study instance generation and the performance comparison of GAGA and the branch and bound algorithm are detailed in Sections 6.3.1 and 6.3.2.

Instance			GAGA-SA-1000		GAGA-SA-10000		GAGA-Yens		Branch-And-Bound	
n	p	i	obj	time (s)	obj	time (s)	obj	time (s)	obj	time (s)
20	0.5	0	2.83 e+06	2931.32	2.64 e+06	4368.71	2.69 e+06	3697.60	4.03 e+06	14400
20	0.5	1	1.45 e+06	2387.13	1.47 e+06	3463.57	1.42 e+06	2390.27	2.15 e+06	14400
20	0.5	2	0.71 e+06	1931.70	0.73 e+06	2503.33	0.75 e+06	1813.50	9.50 e+05	14400
20	0.5	3	2.18 e+05	1625.86	2.09 e+05	2383.20	2.15 e+05	1406.08	3.12 e+05	14400
20	0.5	4	7.39 e+05	2788.98	7.71 e+05	2917.41	8.37 e+05	2186.68	8.35 e+05	14400
20	0.5	5	0.96 e+06	2011.54	0.97 e+06	2678.38	0.90 e+06	1676.48	1.07 e+06	14400
20	0.5	6	3.24 e+06	2536.07	2.89 e+06	3327.69	2.65 e+06	2685.08	3.95 e+06	14400
20	0.5	7	2.08 e+05	2199.30	2.01 e+05	3456.32	2.03 e+05	2229.30	2.56 e+05	14400
20	0.5	8	2.43 e+05	1641.64	2.42 e+05	2354.32	2.41 e+05	1514.79	3.37 e+05	14400
20	0.5	9	6.20 e+05	2529.35	6.24 e+05	3374.94	5.80 e+05	2948.75	5.51 e+05	14400
20	0.75	0	6.90 e+04	1783.51	7.30 e+04	3277.64	7.30 e+04	1188.81	7.86 e+04	14400
20	0.75	1	1.12 e+05	1900.06	1.12 e+05	3649.95	1.12 e+05	1753.16	1.18 e+05	14400
20	0.75	2	0.83 e+05	1691.69	0.87 e+05	2724.63	0.88 e+05	1159.22	1.01 e+05	14400
20	0.75	3	7.00 e+04	2235.44	7.50 e+04	2782.49	7.90 e+04	1148.20	9.35 e+04	14400
20	0.75	4	0.99 e+05	1735.64	1.00 e+05	2965.26	1.02 e+05	1159.36	1.06 e+05	14400
20	0.75	5	0.97 e+05	1963.95	0.97 e+05	3402.85	0.97 e+05	2020.67	1.01 e+05	14400
20	0.75	6	0.91 e+05	1508.97	0.93 e+05	3555.80	0.92 e+05	1476.82	9.74 e+04	14400
20	0.75	7	0.89 e+05	1710.47	0.89 e+05	3122.01	0.90 e+05	1367.58	1.01 e+05	14400
20	0.75	8	0.98 e+05	1776.35	0.99 e+05	3183.02	1.01 e+05	2031.30	1.11 e+05	14400
20	0.75	9	0.99 e+05	1779.24	1.02 e+05	4046.86	1.02 e+05	1470.36	1.05 e+05	14400
30	0.5	0	1.97 e+05	8131.35	1.97 e+05	9303.11	1.84 e+05	6661.51	1.98 e+05	14400
30	0.5	1	2.09 e+05	6741.38	2.05 e+05	8337.86	2.06 e+05	6223.99	2.36 e+05	14400
30	0.5	2	1.62 e+05	6310.00	1.63 e+05	5466.08	1.61 e+05	2403.93	1.80 e+05	14400
30	0.5	3	1.76 e+05	7258.44	1.77 e+05	8490.38	1.83 e+05	5364.12	2.38 e+05	14400
30	0.5	4	3.04 e+05	8005.14	3.22 e+05	8665.91	2.89 e+05	6750.19	3.49 e+05	14400
30	0.5	5	1.88 e+05	7435.17	1.88 e+05	7963.70	1.91 e+05	4415.26	2.26 e+05	14400
30	0.5	6	1.88 e+05	7244.06	1.95 e+05	8679.78	1.88 e+05	5036.13	2.33 e+05	14400
30	0.5	7	3.82 e+05	8138.68	4.05 e+05	9202.13	4.20 e+05	460.71	4.39 e+05	14400
30	0.5	8	1.51 e+05	5786.28	1.52 e+05	7515.79	1.57 e+05	4728.17	1.86 e+05	14400
30	0.5	9	2.78 e+05	7180.90	2.73 e+05	7172.85	2.59 e+05	4259.48	3.30 e+05	14400
30	0.75	0	1.04 e+05	5948.39	1.02 e+05	11937.47	1.05 e+05	3976.56	1.15 e+05	14400
30	0.75	1	1.23 e+05	5546.67	1.22 e+05	10765.75	1.28 e+05	3371.02	1.37 e+05	14400
30	0.75	2	0.98 e+05	7392.68	0.96 e+05	12556.06	1.01 e+05	3642.89	1.14 e+05	14400
30	0.75	3	1.03 e+05	6083.00	0.99 e+05	12773.28	1.04 e+05	2800.32	1.08 e+05	14400
30	0.75	4	0.98 e+05	6049.69	0.95 e+05	12036.30	1.02 e+05	3160.86	1.15 e+05	14400
30	0.75	5	1.04 e+05	6026.44	1.02 e+05	13553.03	1.06 e+05	3695.71	1.13 e+05	14400
30	0.75	6	0.99 e+05	6660.11	0.98 e+05	11316.65	0.99 e+05	3509.40	1.11 e+05	14400
30	0.75	7	1.07 e+05	6519.37	1.05 e+05	11515.46	1.09 e+05	3668.31	1.27 e+05	14400
30	0.75	8	0.93 e+05	6524.25	0.94 e+05	11144.66	0.96 e+05	3562.64	1.06 e+05	14400
30	0.75	9	0.89 e+05	7337.74	0.88 e+05	12763.55	0.93 e+05	4114.14	1.04 e+05	14400

Table 3: Results on random instances with n nodes randomly generated in $U(0,1)$, p probability of an edge with an additional factor based on distance, i instance number. An additional $\frac{n}{10}$ nodes are marked as exits on the boundary of the unit square. These also serve as FR entry points. Capacities of edges are $N(50,20)$. All edges have two lanes in both directions. The population at each node to exit follows a $N(100,10)$. For each instance, the entry for the method with the best performance is in bold text.

Instance	GAGA-SA-10000			GAGA-Yens			Branch-And-Bound	
n_{paths}	n_{graver}	obj	time (s)	n_{graver}	obj	time (s)	obj	time (s)
20	10096	1.23 e+05 (1.24 e+05)	8850.87 (7224.89 + 138.48 + 1321.51 + 165.99)	7432	1.30 e+05 (3.99 e+05)	1662.32 (201.57 + 127.22 + 1176.85 + 156.67)	1.41 e+05	14400
25	15854	1.22 e+05 (1.24 e+05)	10763.01 (7224.89 + 833.29 + 2442.32 + 161.50)	11484	1.25 e+05 (2.81 e+05)	3727.72 (201.57 + 584.36 + 2781.59 + 160.19)		
30	22942	1.22 e+05 (1.23 e+05)	14547.90 (7224.89 + 3058.06 + 4102.57 + 162.37)	16187	1.28 e+05 (2.67 e+05)	6534.44 (201.57 + 1907.81 + 4260.08 + 164.97)		
35	31382	1.23 e+05 (1.24 e+05)	22431.84 (7224.89 + 8714.43 + 6333.83 + 158.67)	22019	1.28 e+05 (1.91 e+05)	14720.39 (201.57 + 5160.53 + 9764.47 + 165.97)		
40	41065	1.22 e+05 (1.23 e+05)	38294.72 (7224.89 + 20923.10 + 9986.53+160.18)	27886	1.29 e+05 (1.82 e+05)	26939.96 (201.57 + 11832.86 + 14740.83+164.69)		

Table 4: For a single graph instance ($n = 30, p = 0.75, i = 1$), comparison between simulated annealing with 10000 samples (GAGA-SA-10000) and Yens k-shortest path method (GAGA-Yens) with a varying number of paths ($k = 20, 25, 30, 35, 40$). The quantity in brackets of the column labeled, "obj" of GAGA-SA-10000 and GAGA-Yens refers to the solution at the end of the GAGA run only (i.e., GAGA-only solution). The time taken for each method of the GAGA algorithm (feasible solutions calculation, Graver basis computation, Graver walk, and *LeBlanc* algorithm) are respectively shown in the brackets of the "time(s)" column.

Instance			GAGA-SA-10000/GAGA-Yens
Initial seed Generator	Graver generator	n_{graver}	obj
SA	SA	15854	1.23 e+05 (1.23 e+05)
Yens	SA	15854	1.25 e+05 (1.36 e+05)
Yens	Yens	22019	1.28 e+05 (1.91 e+05)
SA	Yens	22019	1.25 e+05 (206.17 e+05)

Table 5: For a single graph instance ($n = 30, p = 0.75, i = 1$), comparison between simulated annealing (GAGA-SA-10000) and Yen's k-shortest paths (GAGA-Yens) with the same initial conditions and Graver basis interchanged. The quantity in brackets of the column, "obj" refers to the solution at the end of the GAGA run only (GAGA-only solution).

6.3.1 Instance generation

To demonstrate the impact of FR lane reservation decisions on evacuees' travel times, we designate a realistic case study on a specific region in Istanbul, including the Avcilar district and a neighborhood around the Küçükçekmece Lake. Istanbul is subject to major earthquake risk due to the fault line passing under the sea to the city's south [13], and Avcilar is one of the most risky areas. The region of study is home to nearly 500,000 residents [44].

To generate the region's road network, we leveraged Istanbul's OpenStreetMap (OSM) dataset, focusing on the road infrastructure information layer. This layer is analyzed in ArcGIS 10.5, where links are systematically classified into two groups based on their road-type features. Among the 15 distinct features for road records, the first class encompasses links with road-type features such as *primary*, *secondary*, *motorway*, and *trunk*. These links are precisely mapped in the network and hold the potential for hosting an FR lane reservation. On the other hand, the second class includes lanes with *tertiary*, *residential*, *service*, *track*, and *living street* road-type features. While these links cannot accommodate FR lane reservations due to capacity and lane limitations, they

remain accessible for evacuees and FRs to navigate the network. Given the substantial number of links falling into the second class, the selected arcs comprise only main roads featuring two or more lanes on both sides. Finally, link types such as *cycleway*, *pedestrian*, *footway*, *steps*, and *path* are excluded from the network, as they are impassable for both evacuees and FRs. The resulting network, depicted in Figure 2, consists of 179 vertices, each representing a residential area or an origin node for the FRs, and 234 arcs representing the road infrastructure connecting the vertices in both directions. The thick pink and the thin grey links correspond to the first and second categories of edges, respectively. The yellow patches represent exit nodes. An exit node situated within the region indicates a safe area.

[53] studied a cross-comparative analysis of individuals’ evacuation behaviors in a post-earthquake situation. The authors investigated the GPS trajectories of more than one million anonymized mobile phone users whose positions were tracked for two months before and after four of the major earthquakes that occurred in Japan. They argued that in the face of an earthquake with a 7 seismic intensity, nearly 60% of individuals strive to evacuate the region immediately. This result is, however, regardless of the earthquake hitting time, which can affect the magnitude of the evacuation. Therefore, jointly considering such an evacuation ratio with uncertainties in evacuees’ travel volume, we generated three instances on the same network by varying the evacuation demand level. Based on the population size p_i at each node i provided in the [24] report, 4-person vehicle capacities, and the evacuation ratio reported by [53], we assume among the three instance sets 1, 2, and 3, the number of evacuating vehicles d_i emanating from each demand node i is measured by $\lfloor 0.25p_i \times U[0.1, 0.3] \rfloor$, $\lfloor 0.25p_i \times U[0.3, 0.5] \rfloor$, and $\lfloor 0.25p_i \times U[0.5, 0.7] \rfloor$, respectively. These uniform distributions U account for demand randomness and capture different evacuation ratios depending on the occurrence time of an earthquake with a seismic intensity of 7.

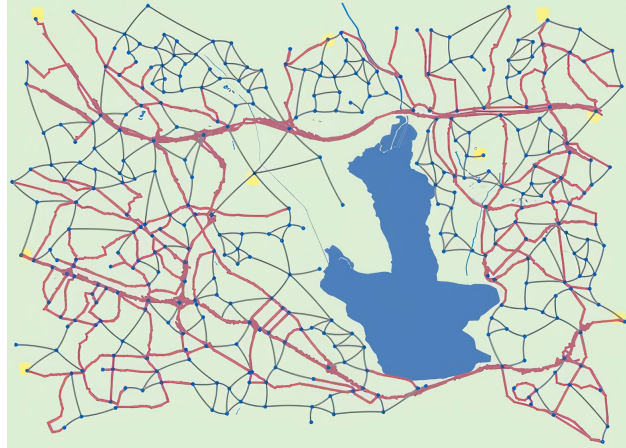


Figure 2: The network associated with our case study instances. FR lanes can be reserved along the thick pink edges. The yellow circles stand for exit nodes.

6.3.2 Comparing GAGA and BB

Within the designated network in Section 6.3, there exists 154 nodes with evacuation demand and 69 nodes with FR demands, varying in demand levels. We generate feasible paths from each demand node to the exit nodes, taking into account the traffic equilibrium. Subsequently, we construct the partial Graver basis for both FR and evacuee paths. We compare the GAGA results using the ‘GAGA-SA-10000’ results with the branch-and-bound results. In the GAGA algorithm, four different settings are explored, as discussed below.

- *Unnormalized*: The evacuee demand is fixed as it is. The Graver walk in the inner user-equilibrium problem is terminated only when no further augmentation is possible at that solution.
- *Unnormalized, Tol = 1e-3*: The evacuee demand is fixed as it is. The Graver walk in the inner problem is terminated when the fractional difference in optima before and after one full pass over all the Graver elements is less than 10^{-3} .
- *Normalized*: The evacuee demand is normalized such that the maximum demand at any node is 100. The optimization in the inner problem is terminated only when no further augmentation is possible at that solution.
- *Normalized, Tol=1e-3*: The tolerance before and after one full pass over all the Graver elements is less than 10^{-3} .

The Branch-and-Bound (BB) algorithm is run up to 72 hours. The Graver walk step in the GAGA algorithm is also given a time limit of 72 hours. Except for the *Unnormalized* setting, the total run time of GAGA for the remaining 3 settings is less than that of BB for all the 3 instances. For the *Unnormalized* setting, the total run time for the 1st instance is less than that of BB. In the remaining 2 instance, we find that the Graver augmentation time increases due to increased evacuee demand. Hence, the Graver walk is not fully completed within the specified time limit for all the initial seeds. We note that all the runs for these instances have been performed on Processor-G.

The results comparing each of the 4 settings and comparing with Branch-and-Bound are tabulated in Tables 6, 7, 8, 9. The run times for each of the three instances are plotted in Figures 3, 4, 5. In all the figures, there is a pre-Graver-walk time for each of the 4 settings to compute the feasible solutions and partial Graver basis. The BB run instead starts from $t = 0s$.

In each figure, the top panel shows the time to solution and the optimal solution at that time, following the order of initial seeds generated randomly from the Simulated annealing solutions. The bottom panel shows the same results but follows the “worst case” ordering where the seed with the worst optimal solution comes first, and the optimal solution decreases as we proceed to the next seeds.

In Figure 3, we show the results for the first instance. We can see that the optimal solution from Branch and bound is similar to the GAGA result for the *Unnormalized* and *Normalized* settings, but larger than the results when including a tolerance threshold setting by $\sim 10\%$. Comparing amongst the GAGA runs, we notice that the time to solution is much longer for the *Unnormalized* and *Normalized* setting with no tolerance setting. The best solution is obtained in the *Unnormalized* setting with a tolerance threshold setting included. This setting requires much less time and is also comparable to the Normalized setting with a tolerance threshold. In Figure 4 and Figure 5, we show the same results for the 2nd and 3rd instances. We again find that the best GAGA results are obtained with the *Unnormalized* and *Normalized* settings with a tolerance threshold and are better than BB by 5% and 20% respectively for the two instances. The BB results are similar to the GAGA runs with only the *Unnormalized* and *Normalized* settings. So, we can conclude that running the GAGA algorithm in an *Unnormalized* or *Normalized* and including a tolerance criterion in the inner user equilibrium problem tends to produce better quality solutions when compared to BB and in a shorter time interval.

Instance			GAGA-SA-10000		Branch-And-Bound	
n	m	l	obj	time (s)	obj	time (s)
179	234	1	1.54 e+06 (M=100)	236438.77	1.55 e+06	259200
179	234	2	2.56 e+07 (M=85)	303312.19	2.56 e+07	259200
179	234	3	1.16 e+08 (M=43)	301813.49	1.23 e+08	259200

Table 6: Comparison of the solution output by GAGA and time to solution with Branch-And-Bound on 3 Turkish graph instances (Avcilar graph with different demands). The GAGA algorithm is run in the *Unnormalized* setting without any normalization of evacuee demand, and there is no adjustment of tolerance in the inner problem.

Instance			GAGA-SA-10000		Branch-And-Bound	
n	m	l	obj	time (s)	obj	time (s)
179	234	1	1.55 e+06 (M=100)	166784.54	1.55 e+06	259200
179	234	2	2.59 e+07 (M=100)	195092.25	2.56 e+07	259200
179	234	3	1.13 e+08 (M=100)	244233.26	1.23 e+08	259200

Table 7: Comparison of the solution output by GAGA and time to solution with Branch-And-Bound on 3 Turkish graph instances (same as in Table 6) with the GAGA run with *Normalized* setting. The maximum evacuee demand in each instance is normalized to 100, and an equivalent factor reduces capacity before Graver walks. There is no adjustment to tolerance in the inner problem.

Instance			GAGA-SA-10000		Branch-And-Bound	
n	m	l	obj	time (s)	obj	time (s)
179	234	1	1.43 e+06 (M=100)	97055.87	1.55 e+06	259200
179	234	2	2.46 e+07 (M=100)	99077.13	2.56 e+07	259200
179	234	3	1.01 e+08 (M=100)	140761.56	1.23 e+08	259200

Table 8: Comparison of the solution output by GAGA and time to solution with Branch-And-Bound on 3 Turkish graph instances (same as in Table 6) with the GAGA run with *Unnormalized*, $Tol = 1e-3$ setting. There is no normalization of evacuee demand, and the criterion for Graver walk termination in the inner user equilibrium level is a tolerance threshold of 10^{-3} .

Instance			GAGA-SA-10000		Branch-And-Bound	
n	m	l	obj	time (s)	obj	time (s)
179	234	1	1.50 e+06 (M=100)	95280.47	1.55 e+06	259200
179	234	2	2.46 e+07 (M=100)	98936.04	2.56 e+07	259200
179	234	3	1.03 e+08 (M=100)	118397.11	1.23 e+08	259200

Table 9: Comparison of the solution output by GAGA and time to solution with Branch-And-Bound on 3 Turkish graph instances (same as in Table 6) with the GAGA run with *Normalized*, $Tol = 1e-3$ setting. Here, the maximum evacuee demand in each instance is normalized to 100, and an equivalent factor reduces capacity before Graver walks. The criterion for Graver walk termination in the inner problem is a tolerance threshold of 10^{-3} .

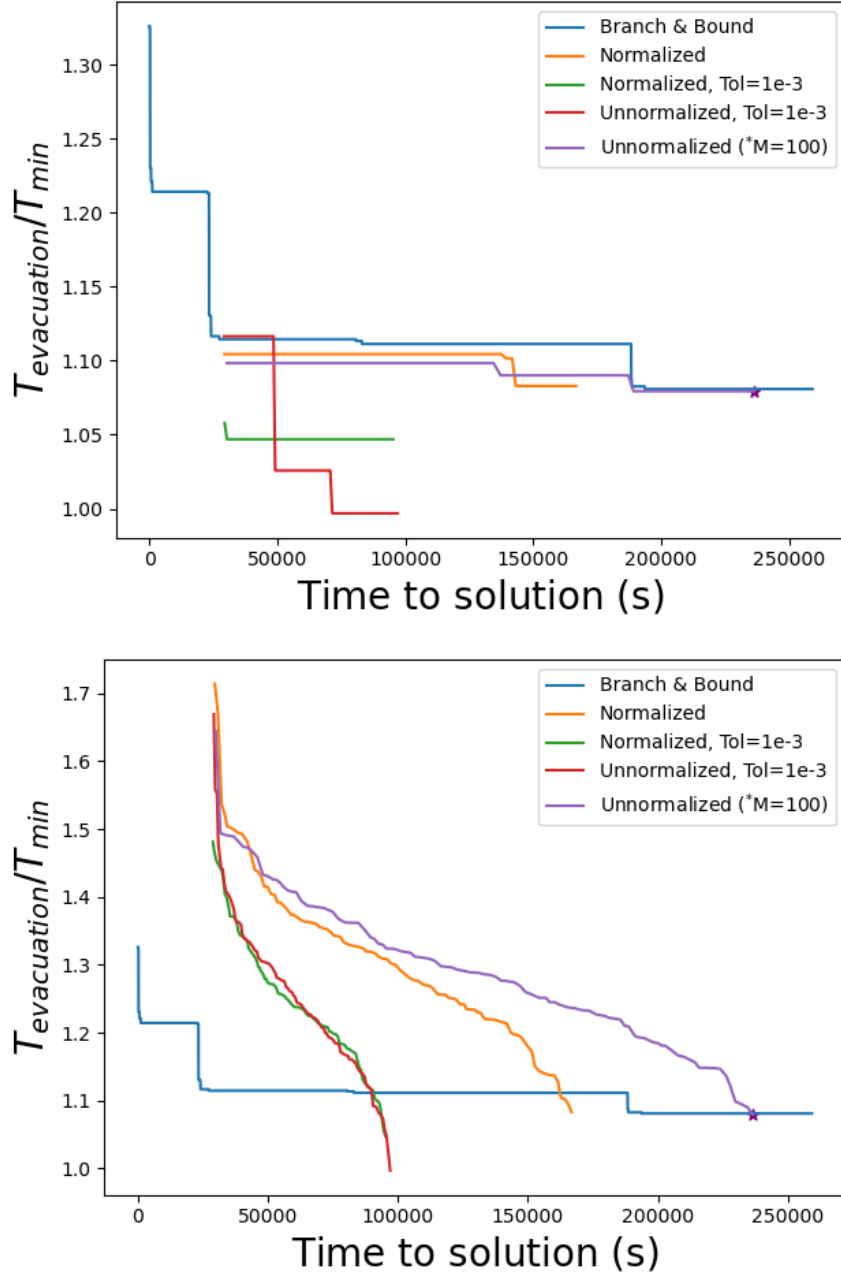


Figure 3: The evacuation times as a function of time to solution for Turkish Graph Instance-1 computed using Graver walk with varying settings (on evacuee demand normalization and tolerance threshold in inner user equilibrium problem) compared against Branch and Bound solution. For each run, the final FR paths (local optimal solutions for each seed) obtained after the Graver walk are all found to be unique. On average, the inner user-equilibrium level with tolerance threshold is faster by a factor of ~ 3.85 than without for the *Unnormalized* setting and ~ 2.5 for a *Normalized* setting. *Top panel:* The best solution at the given time with the order of the seeds is the same as in the computational experiment. *Bottom panel:* The order of seeds is based on the decreasing order of the objective function.

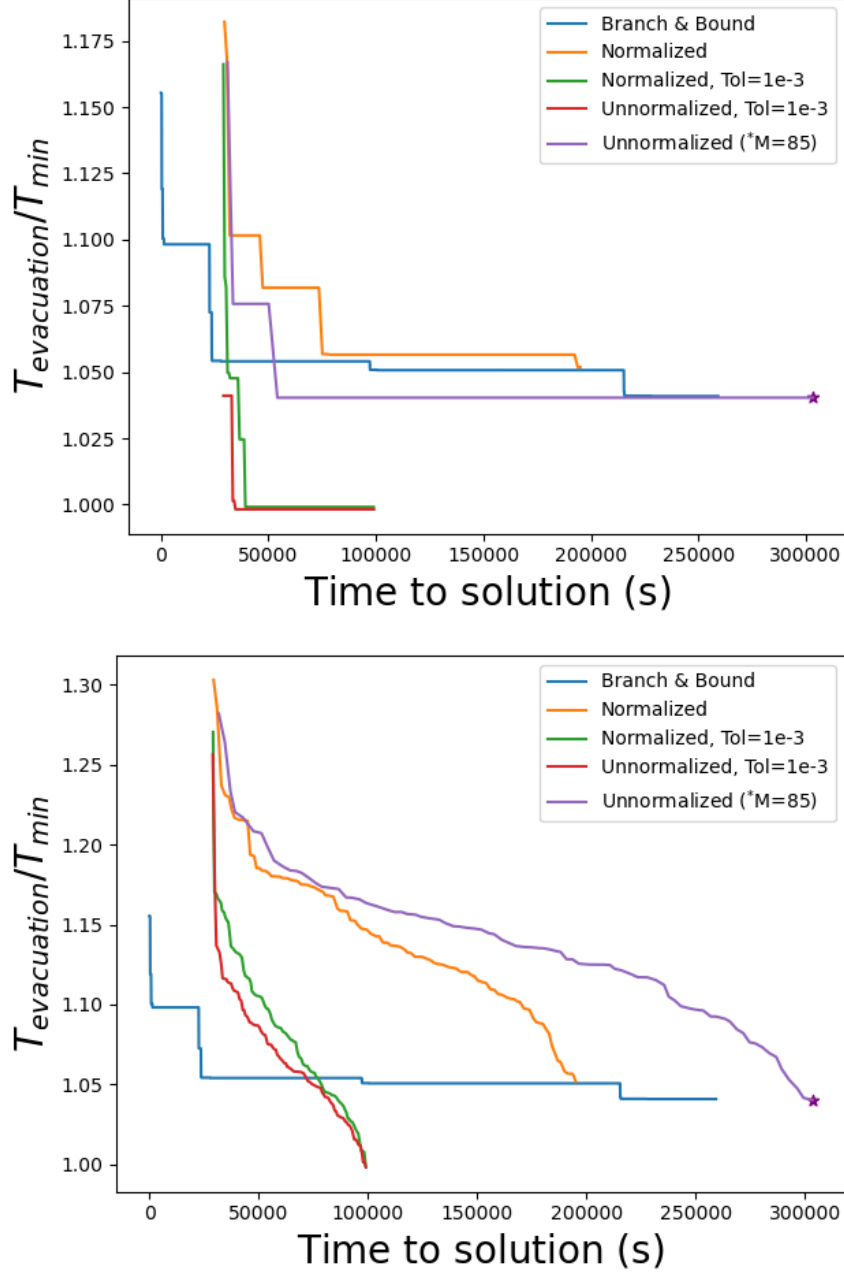


Figure 4: The evacuation times as a function of time to solution for Turkish Graph Instance-2 computed using Graver walk with varying settings (on demand normalization and tolerance) compared against Branch and Bound solution. For the GAGA run with *Unnormalized*, only (*M=85) seeds are used due to the time limit. The remaining GAGA runs use 100 seeds. For each run, the final FR paths (local optimal solutions for each seed) obtained after the Graver walk are all found to be unique. On average, the inner user-equilibrium level with tolerance threshold is faster by a factor of ~ 6.1 than without for the *Unnormalized* setting and ~ 3 for a *Normalized* setting.

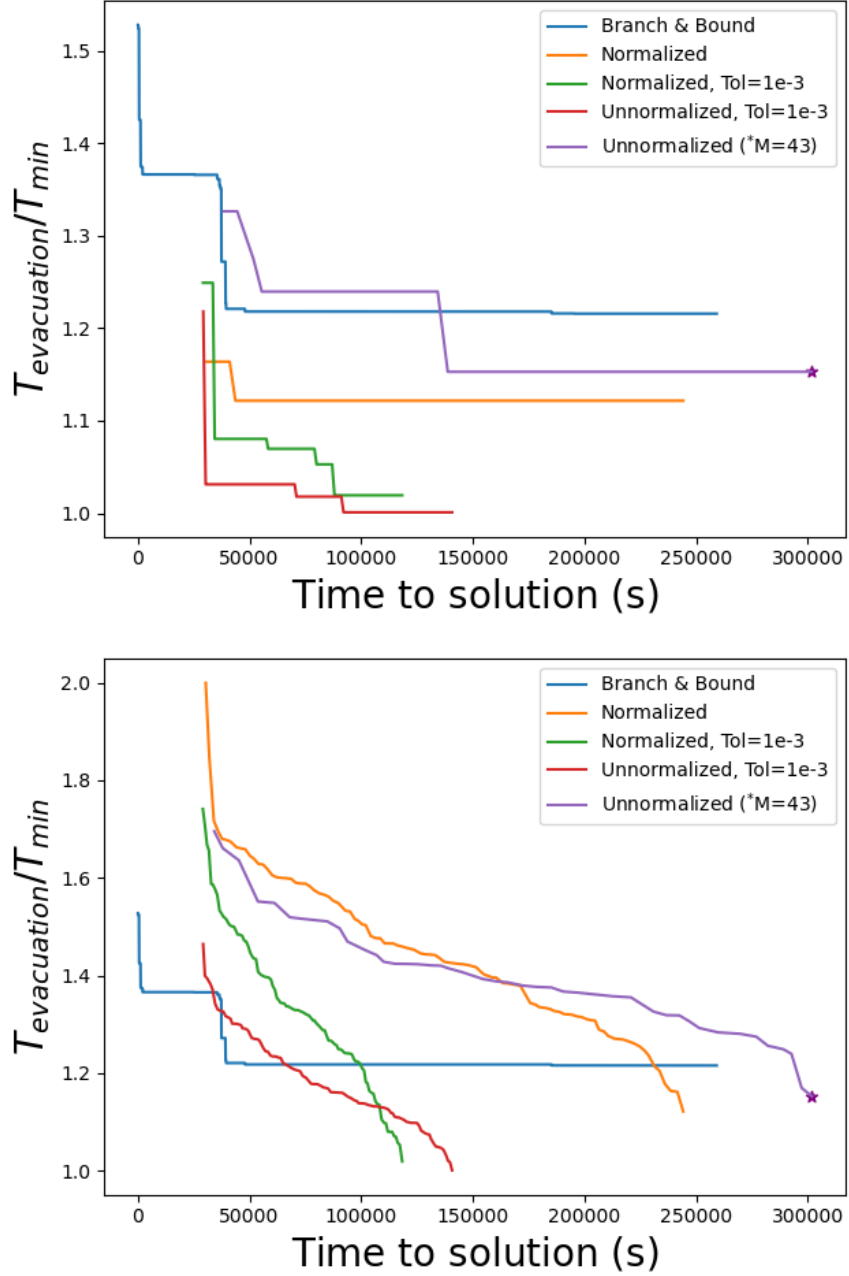


Figure 5: The evacuation times as a function of time to solution for Turkish Graph Instance-3 computed using Graver walk with varying settings (on demand normalization and tolerance) compared against Branch and Bound solution. For the GAGA run with *Unnormalized* setting, only (*M=43) seeds are used due to the time limit. The remaining GAGA runs use 100 seeds. For each run, the final FR paths (local optimal solutions for each seed) obtained after the Graver walk are all found to be unique. On average, the inner user-equilibrium level with tolerance threshold is faster by a factor of ~ 9.56 than without for the *Unnormalized* setting and ~ 3.44 for a *Normalized* setting.

7 Conclusion

Following a disaster, the immediate priority lies in locating and rescuing individuals who may be trapped or injured while ensuring the other entities can travel to safe locations on their own. This is further effective in case the available and restricted lanes are properly labeled, having been pre-determined and pre-communicated. However, identifying such roads requires a careful assessment of the tradeoff between expediting the FR responses and reducing the travel time for the disaster-affected people. This preparedness activity is parallel to other efforts, including establishing medical facilities, providing emergency medical care, and ensuring the availability of crucial medical supplies.

We define the first responder network design problem as a bilevel optimization problem, where the arcs reserved for the first responders are selected at the first level to minimize total travel time, which depends on the second level problem where the public travels between their origin-destination pairs over the eligible roads, adopting a selfish routing principle. We propose a novel solution methodology for this difficult bilevel nonlinear network design problem. Unlike the existing methodologies for similar network design problems, we apply a quantum-inspired algorithm. The algorithm takes advantage of the Graver Augmented Multi-Seed Algorithm (GAMA) and follows a bi-level nested GAMA within the GAMA algorithm that we name GAGA. We test several variations of GAGA on instances related to a set of random graph instances and three scenarios on a predicted Istanbul earthquake. In most instances, we elicit superior solution quality and run-time performance of GAGA compared to a state-of-the-art exact algorithm for a traditional formulation.

We hope that our promising results encourage applying quantum-inspired methods to other disaster preparedness problems with combinatorial aspects and computationally expensive nonlinearity in the objective function and also explore further development of this novel methodology to such complex models in other application domains.

Acknowledgements. ST and AT would like to acknowledge Raytheon BBN for their support through a CMU-BBN contract as part of a DARPA project on Quantum Inspired Classical Computing (QuICC). For AK, this material is also based upon work supported by the National Science Foundation Graduate Research Fellowship Program under Grant No. DGE1745016, DGE2140739. Any opinions, findings, conclusions, or recommendations expressed in this material are those of the author(s) and do not necessarily reflect the views of the National Science Foundation.

Appendix A: Comparison of Processors

Table 10 shows the results of running GAGA on ten instances of a random graph with $n = 30$ and $p = 0.75$ across the two processors. We find that Processor-B is 1.3 times faster, on average, than Processor-G. All reported times in the main body of the paper are unscaled, with GAGA on Processor-G and Branch-And-Bound on Processor-B.

Instance			GAGA-SA-10000-Processor-G		GAGA-SA-10000-Processor-B		Branch-And-Bound	
n	p	i	obj	time (s)	obj	time (s)	obj	time (s)
30	0.75	0	1.02 e+05	11937.47	1.03 e+05	8927.38	1.17 e+05	14400
30	0.75	1	1.22 e+05	10765.75	1.23 e+05	8275.47	1.41 e+05	14400
30	0.75	2	0.96 e+05	12556.06	0.96 e+05	9534.69	1.20 e+05	14400
30	0.75	3	0.99 e+05	12773.28	1.00 e+05	9704.60	1.08 e+05	14400
30	0.75	4	0.95 e+05	12036.30	0.96 e+05	8397.12	1.16 e+05	14400
30	0.75	5	1.02 e+05	13553.03	1.03 e+05	10758.42	1.16 e+05	14400
30	0.75	6	0.98 e+05	11316.65	0.98 e+05	8588.02	1.13 e+05	14400
30	0.75	7	1.05 e+05	11515.46	1.06 e+05	8315.06	1.32 e+05	14400
30	0.75	8	0.94 e+05	11144.66	0.94 e+05	9293.79	1.13 e+05	14400
30	0.75	9	0.88 e+05	12763.55	0.89 e+05	9958.27	1.10 e+05	14400

Table 10: Results comparing processors on $n = 30, p = 0.75$. We find that Processor-B is faster by a factor of ~ 1.3 than Processor-G

References

- [1] Maryam Afkham, Reza Ramezani, and Shahrooz Shahparvari. Balancing traffic flow in the congested mass self-evacuation dynamic network under tight preparation budget: An australian bushfire practice. *Omega*, 111:102658, 2022.
- [2] David A Alexander and Susan Klein. First responders after disasters: a review of stress reactions, at-risk, vulnerability, and resilience factors. *Prehospital and disaster medicine*, 24(2):87–94, 2009.
- [3] Hedayat Alghassi, Raouf Dridi, A Gordon Robertson, and Sridhar Tayur. Quantum and quantum-inspired methods for de novo discovery of altered cancer pathways. *bioRxiv*, page 845719, 2019.
- [4] Hedayat Alghassi, Raouf Dridi, and Sridhar Tayur. GAMA: A Novel Algorithm for Non-Convex Integer Programs. *arXiv e-prints*, page arXiv:1907.10930, July 2019.
- [5] Hedayat Alghassi, Raouf Dridi, and Sridhar Tayur. Graver Bases via Quantum Annealing with Application to Non-Linear Integer Programs. *arXiv e-prints*, page arXiv:1902.04215, February 2019.
- [6] Saeed Asadi Bagloee, Majid Sarvi, and Michael Patriksson. A hybrid branch-and-bound and benders decomposition algorithm for the network design problem. *Computer-Aided Civil and Infrastructure Engineering*, 32(4):319–343, 2017.
- [7] Jonathan F Bard. *Practical bilevel optimization: algorithms and applications*, volume 30. Springer Science & Business Media, 2013.
- [8] Martin Beckmann, Charles B McGuire, and Christopher B Winsten. Studies in the economics of transportation. Technical report, YALE UNIVERSITY PRESS, 1956.
- [9] Jeffrey B. Chou, Suraj Bramhavar, Siddhartha Ghosh, and W Herzog. Analog coupled oscillator based weighted Ising machine. *Scientific Reports*, 9, 2019.
- [10] Stella Dafermos. Traffic equilibrium and variational inequalities. *Transportation science*, 14(1):42–54, 1980.
- [11] J.A. De Loera, R. Hemmecke, S. Onn, U.G. Rothblum, and R. Weismantel. Convex integer maximization via Graver bases. *Journal of Pure and Applied Algebra*, 213(8):1569–1577, 2009. Theoretical Effectivity and Practical Effectivity of Gröbner Bases.
- [12] Duvar English: Turkey’s own independent gazette. Istanbul to be hit by major quake in next 7 years with 64kandilli observatory professor warns. "<https://www.duvarenglish.com/istanbul-to-be-hit-by-major-quake-in-next-7-years-with-64-chance-kandilli-observatory-professor->

- [warns-news-61894#:~:text=Prof.,year%202030%20is%2064%20percent"](#), last accessed 01.15.2024, 2023.
- [13] Mustafa Erdik and Eser Durukal. Earthquake risk and its mitigation in istanbul. *Natural Hazards*, 44:181–197, 2008.
 - [14] Hamid Farvaresh and Mohammad Mehdi Sepehri. A single-level mixed integer linear formulation for a bi-level discrete network design problem. *Transportation Research Part E: Logistics and Transportation Review*, 47(5):623–640, 2011.
 - [15] Hamid Farvaresh and Mohammad Mehdi Sepehri. A branch and bound algorithm for bi-level discrete network design problem. *Networks and Spatial Economics*, 13:67–106, 2013.
 - [16] Pirmin Fontaine and Stefan Minner. Benders decomposition for discrete–continuous linear bilevel problems with application to traffic network design. *Transportation Research Part B: Methodological*, 70:163–172, 2014.
 - [17] Pirmin Fontaine and Stefan Minner. Benders decomposition for the hazmat transport network design problem. *European Journal of Operational Research*, 267(3):996–1002, 2018.
 - [18] Ziyu Gao, Jianjun Wu, and Huijun Sun. Solution algorithm for the bi-level discrete network design problem. *Transportation Research Part B: Methodological*, 39(6):479–495, 2005.
 - [19] Fred W. Glover, Gary A. Kochenberger, and Yu Du. Quantum Bridge Analytics I: a tutorial on formulating and using QUBO models. *4OR*, 17:335 – 371, 2018.
 - [20] James D Goltz and Dennis S Mileti. Public response to a catastrophic southern california earthquake: a sociological perspective. *Earthquake spectra*, 27(2):487–504, 2011.
 - [21] Jack E. Graver. On the foundations of linear and integer linear programming I. *Mathematical Programming*, 9:207–226, 1975.
 - [22] R. Harris, Y. Sato, A. J. Berkley, M. Reis, F. Altomare, M. H. Amin, K. Boothby, P. Bunyk, C. Deng, C. Enderud, S. Huang, E. Hoskinson, M. W. Johnson, E. Ladizinsky, N. Ladizinsky, T. Lanting, R. Li, T. Medina, R. Molavi, R. Neufeld, T. Oh, I. Pavlov, I. Perminov, G. Poulin-Lamarre, C. Rich, A. Smirnov, L. Swenson, N. Tsai, M. Volkmann, J. Whittaker, and J. Yao. Phase transitions in a programmable quantum spin glass simulator. *Science*, 361(6398):162–165, 2018.
 - [23] Raymond Hemmecke, Shmuel Onn, and Robert Weismantel. A polynomial oracle-time algorithm for convex integer minimization. *Mathematical Programming*, 126:97–117, 2011.
 - [24] Istanbul Metropolitan Municipality. Avcilar - deprem ve zemin İnceleme müdürlüğü. "<https://deprenzemin.ibb.istanbul/wp-content/uploads/2020/11/Avcilar.pdf>", last accessed 06.23.2023, 2023.
 - [25] Andrew D King, Juan Carrasquilla, Jack Raymond, Isil Ozfidan, Evgeny Andriyash, Andrew Berkley, Mauricio Reis, Trevor Lanting, Richard Harris, Fabio Altomare, et al. Observation of topological phenomena in a programmable lattice of 1,800 qubits. *Nature*, 560(7719):456–460, 2018.
 - [26] S. Kirkpatrick, C. D. Gelatt, and M. P. Vecchi. Optimization by Simulated Annealing. *Science*, 220(4598):671–680, May 1983.
 - [27] Larry J Leblanc. An algorithm for the discrete network design problem. *Transportation Science*, 9(3):183–199, 1975.
 - [28] Larry J LeBlanc, Edward K Morlok, and William P Pierskalla. An efficient approach to solving the road network equilibrium traffic assignment problem. *Transportation research*, 9(5):309–318, 1975.
 - [29] Jon Lee, Shmuel Onn, Lyubov Romanchuk, and Robert Weismantel. The quadratic Graver cone, quadratic integer minimization, and extensions. *Mathematical Programming*, 136:301–323, 2010.
 - [30] E Brooke Lerner and Ronald M Moscati. The golden hour: scientific fact or medical “urban legend”? *Academic Emergency Medicine*, 8(7):758–760, 2001.

- [31] Paramet Luathep, Agachai Sumalee, William HK Lam, Zhi-Chun Li, and Hong K Lo. Global optimization method for mixed transportation network design problem: a mixed-integer linear programming approach. *Transportation Research Part B: Methodological*, 45(5):808–827, 2011.
- [32] Andrew Lucas. Ising formulations of many NP problems. *Frontiers in Physics*, 2, 2014.
- [33] Peter L. McMahon, Alireza Marandi, Yoshitaka Haribara, Ryan Hamerly, Carsten Langrock, Shuhei Tamate, Takahiro Inagaki, Hiroki Takesue, Shoko Utsunomiya, Kazuyuki Aihara, Robert L. Byer, M. M. Fejer, Hideo Mabuchi, and Yoshihisa Yamamoto. A fully programmable 100-spin coherent Ising machine with all-to-all connections. *Science*, 354(6312):614–617, 2016.
- [34] METU Earthquake Engineering Research Center. *Preliminary Reconnaissance Report on February 6, 2023, Pazarcık Mw=7.7 and Elbistan Mw=7.6, Kahramanmaraş-Türkiye Earthquakes*. Earthquake Engineering Research Center, last accessed 07.01.2024 edition, 2023.
- [35] Naeimeh Mohseni, Peter L McMahon, and Tim Byrnes. Ising machines as hardware solvers of combinatorial optimization problems. *Nature Reviews Physics*, 4(6):363–379, 2022.
- [36] Kazuo Murota, Hiroo Saito, and Robert Weismantel. Optimality Criterion for a Class of Nonlinear Integer Programs. *Oper. Res. Lett.*, 32(5):468–472, sep 2004.
- [37] Nariman Nikoo, Mohsen Babaei, and Afshin Shariat Mohaymany. Emergency transportation network design problem: Identification and evaluation of disaster response routes. *International Journal of Disaster Risk Reduction*, 27:7–20, 2018.
- [38] Srinivas Peeta, F Sibel Salman, Dilek Gunneç, and Kannan Viswanath. Pre-disaster investment decisions for strengthening a highway network. *Computers & Operations Research*, 37(10):1708–1719, 2010.
- [39] Loïc Pottier. The Euclidean Algorithm in Dimension n . In *Proceedings of the 1996 International Symposium on Symbolic and Algebraic Computation*, ISSAC '96, page 40–42, New York, NY, USA, 1996. Association for Computing Machinery.
- [40] David Rey. Computational benchmarking of exact methods for the bilevel discrete network design problem. *Transportation Research Procedia*, 47:11–18, 2020.
- [41] Afshin Shariat Mohaymany and Nariman Nikoo. Designing large-scale disaster response routes network in mitigating earthquake risk using a multi-objective stochastic approach. *KSCE Journal of Civil Engineering*, 24(10):3050–3063, 2020.
- [42] Bernd Sturmfels and Rekha R. Thomas. Variation of cost functions in integer programming. *Mathematical Programming*, 77:357–387, 1997.
- [43] The European Union Delegation in Türkiye, the EU Joint Research Centre. *Türkiye Earthquakes Recovery and Reconstruction Assessment Report, Turkish Presidency Strategy and Budgeting Directorate*. Government of Türkiye, last accessed 07.01.2024 edition, 2023.
- [44] Turkish Statistical Institute (TUIK). Data portal for statistics. "<https://www.tuik.gov.tr/Home/Index>", last accessed 01.11.2024, 2023.
- [45] Office of Planning. Urban Planning Division US Bureau of Public Roads. *Traffic assignment manual for application with a large, high speed computer*. US Department of Commerce, 1964.
- [46] Davide Venturelli and Alexei Kondratyev. Reverse quantum annealing approach to portfolio optimization problems. *Quantum Machine Intelligence*, 1(1-2):17–30, 2019.
- [47] David ZW Wang, Haoxiang Liu, and Wai Y Szeto. A novel discrete network design problem formulation and its global optimization solution algorithm. *Transportation Research Part E: Logistics and Transportation Review*, 79:213–230, 2015.
- [48] Shuaian Wang, Qiang Meng, and Hai Yang. Global optimization methods for the discrete network design problem. *Transportation Research Part B: Methodological*, 50:42–60, 2013.

- [49] Tianshi Wang and Jaijeet Roychowdhury. Oim: Oscillator-based Ising machines for solving combinatorial optimisation problems. In *Unconventional Computation and Natural Computation: 18th International Conference, UCNC 2019, Tokyo, Japan, June 3–7, 2019, Proceedings*, page 232–256, Berlin, Heidelberg, 2019. Springer-Verlag.
- [50] Zhe Wang, Alireza Marandi, Kai Wen, Robert L. Byer, and Yoshihisa Yamamoto. Coherent Ising machine based on degenerate optical parametric oscillators. *Phys. Rev. A*, 88:063853, Dec 2013.
- [51] World Bank and Global Facility for Disaster Reduction and Recovery. *Global Rapid Post-Disaster Damage Estimation (GRADE) Report: February 6, 2023 Kahramanmaraş Earthquakes - Türkiye Report*. World Bank, 2023.
- [52] Yingfeng Wu, Chengbin Chu, Feng Chu, and Naiqi Wu. Heuristic for lane reservation problem in time constrained transportation. In *2009 IEEE International Conference on Automation Science and Engineering*, pages 543–548. IEEE, 2009.
- [53] Takahiro Yabe, Yoshihide Sekimoto, Kota Tsubouchi, and Satoshi Ikemoto. Cross-comparative analysis of evacuation behavior after earthquakes using mobile phone data. *PLoS one*, 14(2):e0211375, 2019.
- [54] Jin Y Yen. Finding the k shortest loopless paths in a network. *management Science*, 17(11):712–716, 1971.
- [55] Ruyang Yin, Jiping Xing, Pengli Mo, Nan Zheng, and Zhiyuan Liu. Bo-b&b: A hybrid algorithm based on bayesian optimization and branch-and-bound for discrete network design problems. *Electronic Research Archive*, 30(11):3993–4014, 2022.
- [56] Eda Yücel, F Sibel Salman, and Idil Arslık. Improving post-disaster road network accessibility by strengthening links against failures. *European Journal of Operational Research*, 269(2):406–422, 2018.
- [57] Qiang Zhang, Shi Qiang Liu, and Andrea D’Ariano. Bi-objective bi-level optimization for integrating lane-level closure and reversal in redesigning transportation networks. *Operational Research*, 23(2):23, 2023.
- [58] Tingting Zhang, Chence Niu, Divya Jayakumar Nair, Edward N. Robson, and Vinayak Dixit. Transportation resilience optimization from an economic perspective at the pre-event stage. *Sustainability Analytics and Modeling*, 3:100027, 2023.